Structural and Mechanical Properties of Thin Films of Bovine Submaxillary Mucin versus Porcine Gastric Mucin on a Hydrophobic Surface in Aqueous Solutions

Madsen, Jan Busk; Sotres, Javier; Pakkanen, Kirsi I.; Efler, Petr; Svensson, Birte; Abou Hachem, Maher ; Arnebrant, Thomas; Lee, Seunghwan

Published in:
Langmuir

Link to article, DOI:
10.1021/acs.langmuir.6b02057

Publication date:
2016

Document Version
Peer reviewed version

Structural and Mechanical Properties of Thin Films of Bovine Submaxillary Mucin (BSM) *vs*. Porcine Gastric Mucin (PGM) on a Hydrophobic Surface in Aqueous Solutions

Jan Busk Madsen,[1] Javier Sotres, [2] Kirsi I. Pakkanen,[1] Petr Efler,[1] Birte Svensson,[3] Maher Abou Hachem,[3] Thomas Arnebrant,[2] and Seunghwan Lee[1]*

[1]Department of Mechanical Engineering, Technical University of Denmark

[2]Department of Biomedical Sciences, Faculty of Health and Society, Malmö University, 20506, Malmö, Sweden; Biofilms-Research Center for Biointerfaces, Malmö University, 20506 Malmö, Sweden.

[3]Enzyme and Protein Chemistry, Department of Systems Biology, Technical University of Denmark

*Corresponding author: seele@mek.dtu.dk

KEYWORDS: hydration, film, bovine submaxillary mucin (BSM), porcine gastric mucin (PGM), pH, lubrication

Abstract

The structural and mechanical properties of thin films generated from two types of mucins, namely bovine submaxillary mucin (BSM) and porcine gastric mucin (PGM) in aqueous environment were investigated with several bulk and surface analytical techniques. Both mucins generated hydrated films on hydrophobic polydimethylsiloxane (PDMS) surfaces from

spontaneous adsorption arising from their amphiphilic characteristic. But, BSM formed more elastic films than PGM at neutral pH condition. This structural difference was manifested from the initial film formation processes to the responses to shear stresses applied to the films. Acidification of environmental pH led to strengthening the elastic character of BSM films with increased adsorbed mass, whereas an opposite trend was observed for PGM films. We propose that this contrast originates from that negatively charged motifs are present for both the central and terminal regions of BSM molecule, whereas a similar magnitude of negative charges is localized at the termini of PGM molecule. Given that hydrophobic motifs acting as anchor are also localized in the terminal region, electrostatic repulsion between anchoring units of PGM molecules on nonpolar PDMS surface leads to weakening of the mechanical integrity of the films.

1. Introduction

Mucins are the major macromolecular component of mucus gels and the glycocalyx covering the epithelial lining. Structurally, mucins are determined to contain unglycosylated N- and C-terminal domains and a heavily glycosylated central domain.[1-3] One of the major biological functions of mucus is to act as physical barrier that protects the epithelium from abrasions and hinders pathogens from entering the tissue.[2,4,5] Additionally, cell membrane-tethered mucins have also been shown to play a role in cell signaling via tyrosine phosphorylation triggering, among other things, pathways involved in cellular motility and adhesion.[6]

Apart from being a key component of mucus, mucins are employed to tailor various surface and interfacial properties of engineering systems too, such as surface hydrophilization,[7] antifouling,[8-11] surface coating models for drug delivery systems,[12] and lubrication.[13-18] Many of these studies employed hydrophobic substrates for the adsorption of mucins from aqueous

solutions. Local glycosylation of mucins in the central region along a long polypeptide backbone imparts distinct hydrophilic and hydrophobic characteristics at the central and terminal regions, respectively. Thus, mucins can behave as macromolecular surfactants at the interface of water/hydrophobic substrates. These features are considered to be shared between different mucins. However, mucins are known to be highly adapted to the environment of their origin and mucins with different biological origins may display different compositional and structural features and, therefore, different interfacial properties.

The objective of this study is to characterize the structural and mechanical features of films generated from two different types of mucins, namely bovine submaxillary mucin (BSM) and porcine gastric mucin (PGM). A hydrophobic surface, namely poly(dimethylsiloxane) (PDMS) was employed as substrate since mucin films are expected to form in a straightforward manner in aqueous environment as mentioned above. Additionally, low elasticity of PDMS (elasticity modulus, 1 – 2 MPa range) allows for soft contacts, which have high relevance in bioengineering applications. BSM and PGM have been employed in a broad range of bioengineering interface science studies,[7-17] partly due to their commercial availability. However, no criteria of selecting one type of mucin, e.g. BSM[7-12,16,17] or the other, i.e. PGM,[13-15] has been established in literature. In fact, even their differences as coating materials have not been addressed in an explicit manner to date. In this study, an array of bulk and surface analytical techniques was employed with the aim to elucidate the differences between the two types of mucin films. In the design of this study, the following points were particularly taken into account. Firstly, recent studies have shown that impurities present in commercially available mucins may have a significant impact on their biophysical properties.[16,19,20] Moreover, the nature and amount of these impurities can vary between different batches. Thus, it would be important to keep the amount of impurities as low

as possible. For this reason, an additional purification step i.e., anion exchange chromatography, was performed on commercially available mucin samples.[19] Secondly, as mucins are polyanionic macromolecules with various acidic moieties, intra- and intermolecular interactions can be controlled by varying ambient pH and it can directly affect the structural and mechanical characteristics of the films. Thus, the structural and mechanical characteristics of the two mucin films were characterized at both neutral and acidic pH, from the film formation stage to exposure to shear stresses.

2. Experimental

2.1 Mucins and buffers

BSM (Type I-S, M3895) and PGM (Type III, M1778) were purchased from Sigma Aldrich (Brøndby, Denmark). BSM was purified by means of anion exchange chromatography as described in detail in a previous study.[19] PGM was purified according to the same procedure with BSM.[19] However, due to PGM's higher tendency to form aggregates, additional sterile filtration was performed through 1.2 μm sterile filters (hydrophilic polyethersulfone sterile filters; Pall Corporation, Cornwall, UK) after 5 μm sterile filters, three times each, to clarify the solution. Fractions containing mucins were analyzed by SDS-PAGE and CBB staining, pooled, dialyzed against milliQ grade water and subsequently freeze-dried. The chromatogram (Figure S1) and SDS-PAGE analysis (Figure S2) of PGM can be found in the Electronic Supplementary Information. All samples were stored at –20 °C and desiccated prior to use. Hereafter, "BSM" and "PGM" exclusively refer to the mucins that were further purified according to the procedures described above. In cases where the mucins received from the manufacturer prior to the

purification are referred, they are denoted as “arBSM” or “arPGM” (to represent “as-received” BSM or PGM).

A citrate-phosphate buffer system was employed in order to control the pH of the buffer solutions either at pH 2.4 (0.01 M citrate/0.001 M Na-phosphate) or at pH 7.4 (0.0001 M citrate/0.02 M Na-phosphate) and NaCl to a physiological concentration of 150 mM was added. This buffer system was used all the experiments in this study except for CD spectroscopy where a slight adjustment was necessary (see section 2.3). BSM and PGM samples were dissolved in either buffer prior to use on a nutating mixer to a final concentration of 1 mg/mL, and all the experiments throughout the study were carried out at this concentration. All chemicals used in this study were of laboratory grade and purchased from Sigma Aldrich (Brøndby, Denmark).

2.2 Zeta (ζ) Potential and Dynamic Light Scattering (DLS)

Samples were prepared in 0.22 μm-filtered buffers and zeta (ζ) potentials and hydrodynamic size distribution were measured using a Malvern Zetasizer Nano ZS two angle particle and molecular size analyzer (Malvern Instruments, Worcestershire, UK). The light source is a He-Ne laser at 633 nm and the temperature was set at 25 °C. Disposable folded capillary cell (DTS1070) and Semi-micro cuvettes (PMMA, Plastibrand™) were employed for zeta (ζ) potentials and DLS measurements, respectively. Each sample was measured in triplicates. For the case of DLS, the Malvern Zetasizer software (Version 7.02) was used to analyze the obtained data. All DLS data were plotted according to the intensity distribution of the hydrodynamic diameter (D_h).

2.3 Circular Dichroism (CD) Spectroscopy

Far-UV CD spectra of BSM and PGM solutions were acquired in the region from 240 to 195 nm by employing a rectangular quartz cuvette with 0.5 mm path length (Hellma GmbH & Co. KG, Müllheim, Germany) using Chirascan spectrophotometer (Applied Photophysics Ltd., Surrey, UK). Due to signal interference, the buffer solutions were diluted 1:2 with milliQ grade water. The pHs of the diluted buffers were measured to be pH 3 and 7.4, respectively. Far-UV CD spectra were recorded with a step size of 1 nm, bandwidth of 1 nm, and time-per-point value of 1.5 s. One spectrum was obtained from the averaging of three traces. All samples were measured in triplicate and averaged again, and any background signal from buffer was subtracted.

2.4 Optical Waveguide Lightmode Spectroscopy (OWLS)

OWLS is based on grating-assisted in-coupling of a He-Ne laser into a planar waveguide coating (200-nm thick $Si_{0.25}Ti_{0.75}O_2$ waveguiding layer on 1 mm thick AF 45 glass (Microvacuum Ltd, Budapest, Hungary)). Adsorption of biomolecules from bulk liquid to the interfacing solid surface is measured by monitoring the changes in the refractive index at the vicinity of the solid-liquid interface. This method is highly sensitive out to a distance of ~200 nm from the surface of the waveguide. Experiments were carried out using the OWLS 210 biosensor system (Microvacuum Ltd, Budapest, Hungary).

In order to keep the substrates for OWLS, QCM-D, and the tribology studies consistent, waveguides were coated with a layer of PDMS. The waveguides were spin-coated at 2500 rpm for 15 s initially with an ultrathin layer (ca. 24.3 ± 3.1 nm, determined by scratch test using atomic force microscopy in tapping mode) of polystyrene (Sigma Aldrich, St. Louis, MO) dissolved in HPLC grade toluene at 6 mg/mL. The base and curing agent of a commercial silicone elastomer (Sylgard 184 elastomer kit, Dow Corning, Midland, MI) were dissolved in

hexane at a ratio of 10:3 (final concentration, 0.5 % w/w). A subsequent ultrathin layer of PDMS (ca. 16.4 ± 0.2 nm)[21] was then added by spin-coating at 2 000 rpm for 25 s and cured in an oven at 70 °C overnight.

The PDMS-coated waveguide was exposed to the appropriate buffer prior to sample injection until a stable baseline was obtained. A programmable syringe pump (Model 1000-NE, New Era Pump Systems, Inc., NY) was used to pump buffer solutions through a flow-cell over the OWLS waveguide surface. Sample (100 μL) was then injected via a loading loop. Upon observing surface adsorption, the pump was stopped so that the BSM or PGM molecules could adsorb onto the surface under static conditions. After 10 min, the flow cell was rinsed with the appropriate buffer by restarting pumping. The adsorbed mass density data were calculated according to de Feijter's equation.[22] The experiment was repeated two or three times for each mucin at either pH. A refractive index increment (dn/dc) value of 0.150 cm^3/g was used for the calculation of the adsorbed masses.[23]

2.5 Quartz Crystal Microbalance with Dissipation (QCM-D)

QCM-D measurements were performed by using an E4 system (Q-Sense AB, Sweden). A detailed description of the technique and its basic principles can be found elsewhere.[24] Gold-coated quartz sensors (Q-sense AB, Sweden) were coated with an additional PDMS layer in the same manner as described for OWLS waveguide chips. Solutions were supplied into the QCM-D chamber using an Ismatec peristaltic pump IPC-N 4 at a flow rate of 0.2 $mL \cdot min^{-1}$. Buffer solution was first injected into the chamber until a stable baseline was observed. Then, mucin solution was flowed through the chamber until significant adsorption was observed. At this point the flow was stopped and the mucins were left to adsorb for 10 min under non-flow conditions.

Finally, the cell was rinsed for 5 min with the corresponding buffer solution and then stabilized for ca. 10 min under non-flow conditions. Each experiment was performed twice. During the experiments, shifts in frequency, Δf_n, and dissipation factor, ΔD_n, for the different overtones (n = 3, 5, 7, 9, and 11) were monitored.

In QCM-D experiments, the PDMS-coated sensors were oscillated by applying an alternating-current voltage across it. The raw experimental data provided by QCM-D consist of shifts in the resonance frequencies of the sensor, Δf_n where n is the overtone number, and in the dissipation factor, ΔD_n, which is proportional to the ratio between the dissipated and the stored energy during a single oscillation. Adsorption of a certain amount of mass onto the sensor surface leads to a decrease in the frequency of the resonance overtones,[25] although it is not straightforward to establish the correct relationship between both quantities when dealing with viscoelastic materials.[26] Additionally, the coupled mass sensed in QCM-D experiments includes that of the adsorbed film and that of the coupled solvent.[27,28] Thus, it is often referred as "wet mass". QCM-D also provides information on the viscoelasticity of the adsorbed films. This is usually inferred from dissipation shifts. However, it is not straightforward to quantify the viscoelastic character as dissipation shifts are associated not only with the viscoelasticity of the adsorbed material but also with changes in wet mass.[29] Still, a simple way to qualitatively describe the viscoelasticity of the adsorbed material is to analyze the ratio between frequency and dissipation shifts, $\Delta D/\Delta f$, higher absolute values suggesting a higher viscous character.[30]

2.6 Pin-on-Disk (PoD) Tribometry

The lubricating properties of BSM and PGM films were investigated with a pin-on-disk tribometer (CSM, Peseux, Switzerland). This approach is based on a loaded pin forming a sliding

contact with a disk. A pin on a disk contact was generated in mucin solutions (1 mg/mL) in variation of type (BSM or PGM) and pH (7.4 or 2.4). The load on the pin was controlled by the application of dead weight (1 N). The friction forces between them were measured at incrementing speeds of the disk from 0.25 mm/s to 100 mm/s. Thus, the coefficient of friction (μ) vs. speed plots were acquired. Disk rotation was enabled by a motor beneath the disk while the pin remained stationary. Friction generated during sliding contacts was monitored by a strain gauge. Friction forces data were acquired over 20 rotations at a fixed radius of 5 mm. A PDMS-PDMS tribopair was used for the experiments. PDMS was prepared by thoroughly mixing base fluid and crosslinker of a Sylgard 184 elastomer kit (Dow Corning, Midland, MI) at a ratio of 10:1. Gentle vacuum was applied to remove air bubbles generated during mixing. The disks were prepared by casting the PDMS mixture into a home-machined aluminum plate with flat wells designed to the dimensions (30 mm diameter × 5 mm thickness) of the tribometer. A 96 microwell plate (NUNCLON Delta Surface, Roskilde, Denmark) with a hemispherical end (∅ = 6 mm) was used as a mold for casting the pin. The PDMS mixtures were cured at 70 °C overnight.[15,17]

3. Results and Discussion

3.1 Charge characteristics and hydrodynamic size and charge characteristics of mucins: ζ potential and DLS

In Figure 1, the ζ potentials and hydrodynamic diameter, D_h, distribution of BSM and PGM according to intensity at pH 7.4 and 2.4 are presented.

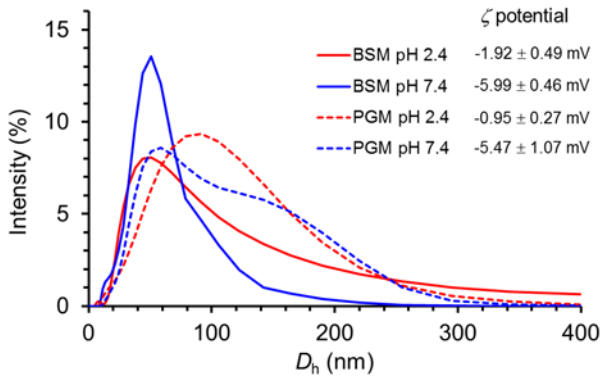

Figure 1. Hydrodynamic size, D_h, distribution of BSM (solid lines, blue for pH 7.4 and red for pH 2.4) and PGM (dotted lines, blue for pH 7.4 and red for pH 2.4) at neutral and acidic pH as characterized by DLS (intensity-weighted). ζ potentials of BSM and PGM solutions at both pHs are also presented.

The ζ potentials of BSM and PGM showed negative values at both pH 7.4 and 2.4, although the magnitude has been greatly reduced at pH 2.4. This is due to the presence of acidic moieties and the protonation of carboxylic groups of sialic acid moieties at pH 2.4. Despite slightly different values, BSM and PGM showed comparable ζ potentials at two pH conditions, which indicates that their overall charge characteristics are fairly similar. However, detailed distribution of charges over BSM and PGM molecules might clearly differ as will be more discussed below.

An important feature in the distribution of D_h after the chromatographic purification of both mucins is that large species ranging from a few hundreds to thousands nm in D_h that were observed from arBSM or arPGM disappeared[19] (D_h distributions for the mucin samples prior to the purification are shown in Figure S3, Supporting Information). Thus, in addition to minimizing non-mucinous protein "impurities" from the samples (see Figure S2), a second effect of the chromatographic purification in this study is to homogenize the size of mucin molecules. As a result, the absolute majority of D_h is less than 200 nm and 300 nm for BSM and PGM, respectively, and the Z-average D_h for BSM and PGM are 56.1 ± 8.9 nm and 77.8 ± 19.7 nm,

respectively, at pH 7.4. As shown in a previous study, the D_h of BSM was only twice as large as that of contour length on average.[31] For this reason, while mucins are often depicted as highly coiled polymer chains in literature,[32,33] the mucins in this study are better described as "dumbbell"-like shape in their conformations.[13,14,34] For instance, a recent small angle x-ray scattering study has revealed that highly purified "Orthana" PGM displays double-globular comb structure with two globules of an average radius of 10 nm connected with the intramolecular chain of ca. 48 nm.[35] At pH 7.4, although the maximum peak positions for BSM and PGM are close to each other, 50.7 nm and 58.8 nm, respectively, the distribution of D_h of PGM is slightly, yet clearly higher than that of BSM. Upon lowering pH to 2.4, the distribution of D_h of both mucins is somewhat shifted to the right (larger values). Shifting pH from 7.4 to 2.4 is expected to protonate the carboxylic acid moieties in mucins as mentioned above, and it can result in two opposing effects in their hydrated sizes. Firstly, due to the reduced intramolecular electrostatic repulsion, which is consistent with lower ζ potential values (Figure 1), D_h can be reduced at low pH.[31] This is a general trend for all charged macromolecules. Secondly, because of the reduced tendency to shield hydrophobic moieties at the unglycosylated terminal domains at low pH, the interaction between exposed hydrophobic patches and consequent aggregation may occur.[36] Figure 1 shows that a slight decrease in D_h with decreasing pH indeed occurs in the main peak of BSM (the most probable peak position shifted from 58.8 nm at pH 7.4 to 50.7 nm at pH 2.4), although the overall increase of D_h at higher range (> 80 nm) is also observed. In contrast, PGM shows an increase in the distribution of D_h only upon shifting pH from 7.4 to 2.4. This difference is ascribed to more abundant presence of negatively charged moieties in the central, glycosylated regions of BSM compared to PGM;[18] the density of negatively charged carbohydrate moieties in the oligosaccharides in BSM (~30% of total carbohydrate mass is sialic acid) has been reported

to be higher than in PGM (2-9% sulphate terminal group modifications) according to previous analysis of the two mucins. [37-41,42] Another study on the compositional analysis of "Orthana" PGM indicated the complete absence of charged glycans.[34] The manufacturer's estimation on the amounts of bound sialic acids is also substantially higher for BSM (ca. 9-17%) than PGM (0.5-1.5%) of the total mucin masses. As the overall size of mucins are determined mainly by the central, glycosylated region than terminal regions,[4,19] higher density of negatively charged motifs in the former for BSM can be directly related to more sensitive changes of D_h distribution according to pH change, even though ζ potentials of the two mucins were determined to be comparable at both pH values (Figure 1).

3.2 Conformation of BSM and PGM: CD spectroscopy

The secondary structures of BSM and PGM were investigated by far UV CD spectroscopy at pH 3 and 7.4 as shown in Figure 2. As mentioned above, for the acidic buffer, the pH was raised to ~3 from the initially targeted pH of 2.4 due to signal interferences.

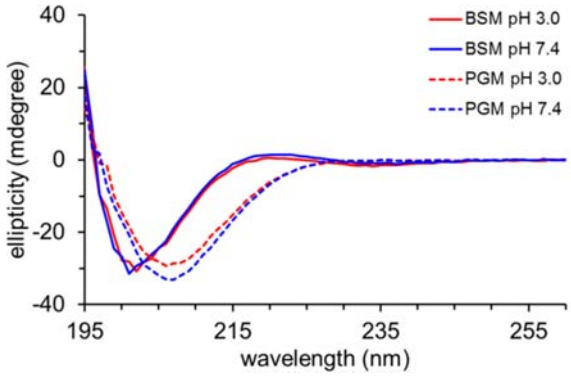

Figure 2. Far-UV CD spectra (260 nm to 195 nm) for BSM (solid lines) and PGM solutions (dash lines) at pH 7.4 (blue) and pH ~3 (red).

The far-UV spectra showed that both BSM and PGM lacked distinct and well defined secondary structures, such as α-helices, β-sheets, or β-turns. [43,44] This is hardly surprising as mucins are mainly made up of the heavily glycosylated 'Proline-Threonine-Serine' (PTS) repeat central domains, and the stiffness of glycans tend to hinder the formation of highly ordered structures.[1, 44-47] Only the N- and C-terminal domains have been assigned to contain structural motifs determined from the peptide sequence, including cysteine knots, CysD domains and Von Willebrand factor binding domains that are involved in mucin-mucin interactions.[1,5,45,48,49] However, the contribution from them to CD spectra signals is not significant due to the dominance of the glycosylated central domain. The far-UV CD spectra of BSM showed a weak, yet distinct local positive maximum at ca. 218 nm and a strong negative minimum at ca. 201 nm. Meanwhile, PGM shows only a single large negative minimum at ca. 207 nm (Figure 2). The features presented by BSM in the far UV range are quite similar to those of poly(Pro) II helices, even though the exact peak positions are somewhat shifted from those observed from poly(Pro) II peptides (where the major peak minimum is observed at 196 nm). [44,50] A most classical view on the secondary structure of proteins as characterized with CD spectroscopy was that any features other than α-helices, β-sheets, or β-turns were grouped together and assigned as "random coil" structure. However, systematic studies with well-prepared poly(Pro) II peptides have shown that polypeptides showing the signals in this region are not entirely disordered, but possess helices arising from proline residues. [50,51] With the presence of a significant number of proline residues in the primary structure of BSM, it is reasonable to propose that secondary structural features pertaining to poly(Pro) II peptides is present in the far-UV CD spectra. The shift of the characteristic peaks compared to poly(Pro) II peptides is ascribed to the heavy glycosylation and further stiffening of the structure of BSM. It is rather intriguing that the far-

UV CD spectra of PGM is quite different from that of BSM and do not display features of poly (Pro) II helical motifs, although PGM also contains central domains made up of the glycosylated tandem repeat PTS-domains. This is also likely related to the glycosylation of the PTS region of PGM, yet different from that of BSM in terms of both types of glycans and the extent, as mentioned above. For instance, the presence of negatively charged groups in the vicinity of nearly every third amino acid residue of BSM may impose further steric constraints on the φ and ψ torsion angles in the polypeptide backbone in addition to the rigidity conferred by proline residues.[51] In comparison, the lower charge density in the central domains of PGM offers relatively higher rotational freedom in the apomucin. It is therefore likely that intramolecular repulsion between the negatively charged oligosaccharides force BSM into a more ordered structure in comparison to PGM. [37-41,52]

For both BSM and PGM, acidification does not seem to affect the far-UV CD spectra, which are dominated the central PTS-domain. This implies that possible conformational changes that occur due to the acidification do not alter the prevalent random coil secondary structure of the proteins. This can be explained by relatively small and homogeneous size distributions of both mucins after the additional purification step and their "dumbbell"-like,[34,35] extended conformation, for which protonation/deprotonation of the acidic moieties along the PTS-domain can hardly affect the conformation of mucins in bulk solution. As the acid-induced aggregation occurs through the interaction between the terminal groups, its influence on the central domains is also expected to be ignorable. For the same reason, however, it is very difficult to determine whether the acidification causes structural changes in the N- and C-terminal domains from far-UV CD spectra. Potential structural rearrangements in the terminal domains of mucins may have

an influence on the surface properties as the interaction with the hydrophobic surface occurs predominantly with those domains, as shown below.

3.3 Surface adsorption: OWLS

Representative adsorption profiles and the average adsorbed masses of the mucins onto PDMS surfaces as characterized with OWLS are presented in Figure 3.

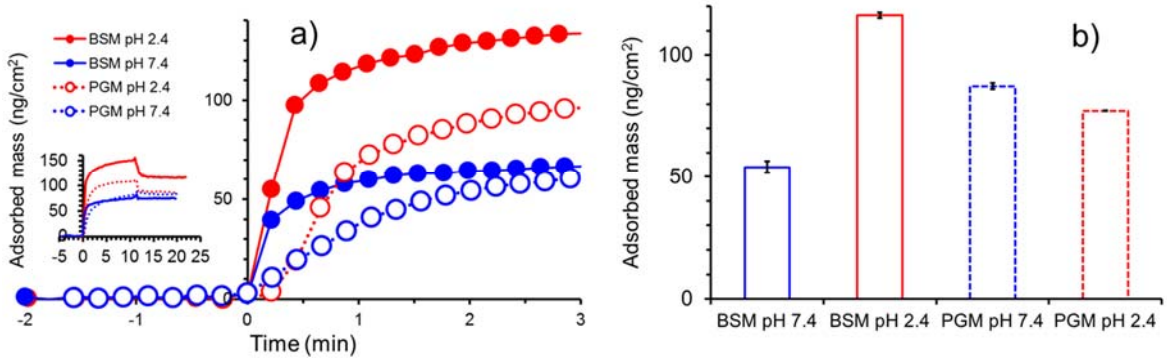

Figure 3. (a) Representative adsorption profiles of BSM and PGM onto PDMS surface at pH 7.4 and 2.4 (b) the average adsorbed masses as characterized by OWLS.

As shown in Figure 3(a), the adsorption of all mucins onto PDMS surface was observed to be slow in the initial stage for both mucins and at both pHs. While *pseudo* equilibrium was reached within 10 min exposure of PDMS surface to mucin solutions, further exposure to mucin solution led to slight, yet continuous increase in the adsorbed mass for all cases (up to 24 hrs, data not shown). In this study, the primary interest was to understand the adsorption behaviour of mucins onto the PDMS surface under tribological stress. As will be further discussed in section 3.3, circular sliding tracks in the pin-on-disk tribometry setup forces the adsorbed mucins films to be rubbed away and new films are repeatedly generated. Thus, the initial stage of surface adsorption

is more relevant to understanding the lubricating properties of mucins films rather than behaviour at equilibrium. For this reason, adsorbed mass was determined by rinsing after 10 min for all cases. At pH 7.4, the adsorbed masses of BSM and PGM onto the PDMS surface were 54 ± 2.4 ng/cm^2 and 87 ± 1.3 ng/cm^2, respectively. Lowering pH from 7.4 to 2.4 significantly increased the adsorbed mass of BSM to 116 ± 1.1 ng/cm^2 whereas slightly decreased to 77 ± 0.1 ng/cm^2 for PGM (Figure 3). A previous study of BSM adsorption onto hydrophobized silica surfaces showed an increase in the surface adsorption at acidic buffer (pH 3.8, 2 mg/mL bulk concentration) too. [53] The increase of the adsorbed mass of BSM at acidic pH is mainly ascribed to the suppressed intra- and intermolecular electrostatic repulsion, and consequently more facilitated packing of BSM molecules on the nonpolar PDMS substrate in aqueous environment. In fact, this is a typical behaviour expected from the adsorption of amphiphilic polyanions onto nonpolar surfaces from aqueous solution.[54,55] As the electrostatic repulsion between neighbouring BSM molecules on surface occurs in a more confined space than in bulk solution, the increase in adsorbed mass (Figure 4) appears to be more enhanced than the increase in the hydrodynamic size distribution (Figure 1).

PGM, on the other hand, showed much less sensitive response to pH change as only a slight decrease in the adsorbed mass (by 11% on average) was observed at pH 2.4 compared to that at pH 7.4. In a previous study, a decrease in the adsorbed mass of arPGM at low pH was attributed to the increase in the hydrodynamic size of arPGM as a result of aggregation;[15] aggregated macromolecules tend to reveal less effective packing on the surface because of the bulkiness. The magnitude of decrease in the adsorbed mass of PGM by acidification in this study is, however, much smaller than that for arPGM,[15] presumably because the increase in D_h at low pH for the purified PGM is also less extensive as shown in Figure 1. Even though an increase in D_h

was observed from BSM too at low pH (Figure 1), the mechanism related to negative charge density on BSM mentioned above may dominate the adsorption properties onto nonpolar PDMS surface and resulted in an increase of the adsorbed mass at low pH.

Lastly, as shown in Figure 3(a), the surface adsorption kinetics in the initial stage (< 3 min) at pH 7.4 is clearly faster for BSM than PGM in the sense that *pseudo* equilibrium is reached faster for the former. Given that adsorption of mucins onto PDMS surface is driven by hydrophobic moieties in the terminal regions, we propose that faster adsorption kinetics of BSM at pH 7.4 may indicate that hydrophobic moieties in BSM are more exposed to solvent and can quickly interact with PDMS surface. In the same context, we can also hypothesize that hydrophobic moieties of PGM are more buried inside the hydrophobic pockets that rearrangement is required to interact with PDMS surface, and thus the surface adsorption process is slowed down. In other words, the difference in surface adsorption kinetics between BSM and PGM at pH 7.4 is closely related to their structural difference related to anchoring motifs onto hydrophobic substrates. The fact that initial surface kinetics of the two types of mucins is fairly similar at pH 2.4 is consistent with this view as the hydrophobic moieties of PGM are also expected to be highly exposed to solvent at acidic environment.

3.4 Surface adsorption and surface viscoelasticity of the mucin films: QCM-D

QCM-D can be complementary to optical approaches in the characterization of macromolecular surface adsorption due to its unique ability to probe not only the solid components adsorbed on the sensor (mucins), but also to the solvent coupled to the sensor.[27] Additionally, the response to the resonance of the adsorbed films can reveal the viscoelastic and mechanical characteristic of the films. The results from QCM-D study are presented in Figure 4.

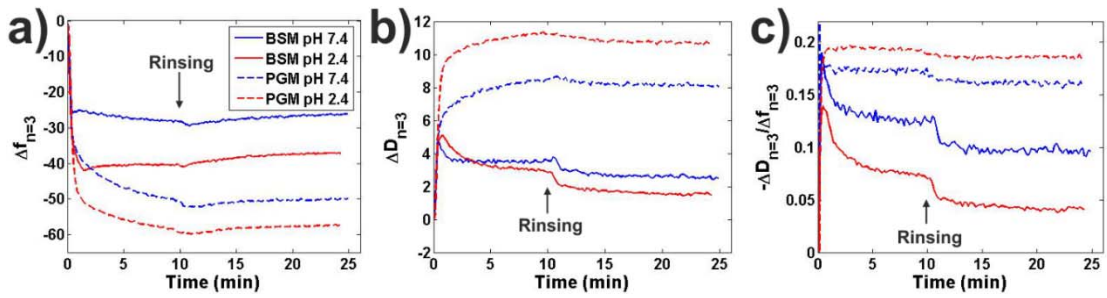

Figure 4. a) Frequency shifts (Δf), b) dissipation shifts (ΔD) and c) $\Delta D/\Delta f$ ratio corresponding to the formation of BSM and PGM films on PDMS surfaces both at pH 7.4 and 2.4 monitored by means of QCM-D. Data corresponds to the 3rd overtone of the sensor. The rest of the monitored overtones showed a similar behaviour.

We first focus on the data collected at pH 7.4. In this case PGM led to films featured with significantly higher shifts in frequency than BSM both before and after being rinsed with protein-free buffer (Figure 4(a)). A higher shift in frequency suggests a higher wet mass coupled to the sensor. Therefore, at pH 7.4 the wet mass follows the same trend as the dry mass, both quantities being higher for PGM than for BSM at PDMS surfaces. Additionally, it has been shown for adsorbed mucin films that the coupled solvent is the main contributor to the wet mass sensed by QCM-D response.[53] Therefore, our data suggests that PGM films are more hydrated than BSM films. Along with frequency shifts, dissipation shifts were also monitored (Figure 4(b)). Dissipation shifts are associated with the viscoelasticity of the adsorbed material, but also with the adsorbed mass. As previously commented, the viscoelasticity from the sample is better inferred from the ratio between the dissipation and frequency shifts. This parameter i.e., $-\Delta D/\Delta f$ (Figure 4(c)), indicates that PGM films have a higher viscous character than BSM films.

Interestingly, shifting the environmental pH from 7.4 to 2.4 had a different effect on the two types of mucin films. The wet mass of both systems i.e., $-\Delta f$, was higher at low pH values. However, $-\Delta D/\Delta f$ followed an opposite trend for both systems. In the case of BSM films, lower

values i.e., more elastic/less viscous character, was observed at pH 2.4 than at pH 7.4. This suggests that the higher "dry mass" observed at low pH is a dominating factor leading to more elastic films. On the contrary, in the case of PGM films, higher $-\Delta D/\Delta f$ values i.e., less elastic/more viscous character, were observed at pH 2.4 than at pH 7.4. The fact that the average D_h of PGM molecules was determined to be somewhat larger (Figure 1) at pH 2.4 than at pH 7.4 and the fact that higher wet mass but lower dry mass was observed at pH 2.4 than pH 7.4 together imply that the formation of a PGM film at pH 2.4 is achieved in a way resulting in more loose structure with more incorporated solvent.

It is worth to note that BSM and PGM films exhibited another difference during the surface adsorption process. In the case of BSM films, an initial overshoot, mostly in the dissipation shift but also slightly in the frequency shift, was observed. Both quantities then followed a gradual decrease at both studied pHs. This is well illustrated in the $-\Delta D/\Delta f$ plot (Figure 4c). This behaviour, which has previously been observed for BSM films formed on hydrophobic substrates, [53,56,57] can be explained by the BSM films capturing a high amount of solvent in the beginning of the adsorption process, which is then gradually released as the film changes into a more compact conformation. On the contrary, PGM films did not exhibit this behaviour. In other words, our data indicates that no significant conformational changes occurred in the formation process of PGM films.

3.5 Resistance to shear stress: Pin-on-disk tribometry

The sliding contacts of PDMS-PDMS interface is known to reveal high interfacial friction forces, mainly due to the high adhesion between two PDMS surfaces in ambient or even in distilled water.[21] But, in aqueous solution of amphiphilic macromolecules, e.g. synthetic block copolymers[21] or mucins,[15-17] spontaneous adsorption and formation of lubricating films by these

macromolecules tend to convert the interface from hydrophobic to hydrophilic, entrain water, and reduce the interfacial friction forces. While the lubricating efficacy is determined by many factors, the stability of lubricating films is most influential. Thus, the lubricating effects by the two types of mucins at PDMS-PDMS interface in this study are expected to provide the additional information on the structural and mechanical characteristics of the films on PDMS surface related to the structure and mechanical stability. Figure 5 shows μ vs. speed plots of PDMS-PDMS sliding contacts in BSM or PGM solutions (1 mg/mL) at pH 7.4 and 2.4.

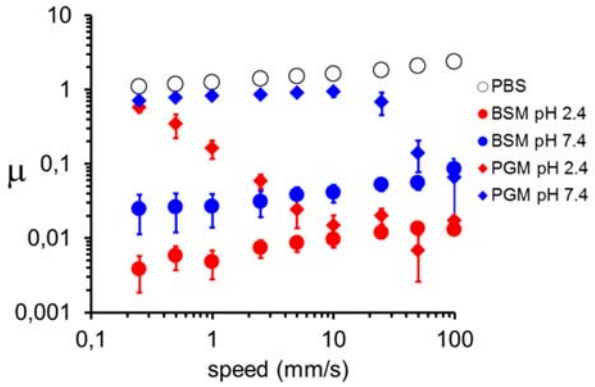

Figure 5. μ vs. speed plot of self-mated sliding of PDMS surfaces lubricated with either 1 mg/mL of BSM (pH 2.4; red circle, pH 7.4; blue circle) or PGM (pH 2.4; red diamond, pH 7.4; blue diamond) or buffer (empty circle).

Overall, superior lubricating properties of BSM to PGM are clearly manifested at both pH conditions, especially in low-speed regime where boundary lubrication is the dominant lubrication mode. BSM solution showed excellent lubricating properties with μ values slightly increasing with increasing speed, ca. from 0.03 to 0.09, at pH 7.4. At pH 2.4, they were further reduced by lowering pH to 2.4. An improvement in the lubricity of BSM at pH 2.4 is well correlated with the transition to more elastic films at pH 2.4, as confirmed by parallel studies of OWLS and QCM-D (Figure 3 and 4).

Meanwhile, the μ values for PGM at pH 7.4 were ca. 0.7 – 0.9 in low-to-mid speed range and were comparable to those of buffer solutions, until the sliding speed reaches 50 mm/s or higher where they started to decrease to ca. 0.15 or lower. At pH 2.4, the μ values of PGM solution was comparable to those of BSM solution at speeds ≥ 10 mm/s, but this lubricating effect started to diminish with decreasing speed. Poor lubricity of PGM films in spite of their highly hydrating capabilities suggests that the large amount of water molecules coupled with the PGM films may be only loosely bound and easily squeezed out from the tribological contacts without contributing to the lubrication of the PDMS-PDMS interface. While hydration of the interface is a commonly demanded attribute for effective aqueous lubrication,[58] its efficacy is further dependent on the tenacity of water molecules coupled within the films at the tribological interface. Moreover, the lubricating properties of PGM film were observed to be improved at pH 2.4 despite its more viscous character ($-\Delta D/\Delta f$ in Figure 4(c)). Compared to BSM films, this behaviour is similar in the net lubricating effect but opposite in the changes of mechanical characteristics. Thus, we propose that the reduced electrostatic repulsion is the dominant factor to drive the improved lubricity of PGM films at pH 2.4.

As discussed above, the lubricating properties of the mucin film are closely related to their structural features as determined by OWLS and QCM-D. Nevertheless, it is also important to note that initially formed mucin films alone are not sufficient to provide persistent lubricating effect under the experimental conditions in this study. For instance, the μ values presented in Figure 5 were obtained from the minimum 20 rotations over the sliding track in pin-on-disk tribometry, and stable μ values were obtained only when excess amount of mucins were present in bulk solution (1 mg/mL in this study). With an initially adsorbed mucin layer alone on PDMS surface in protein-free buffer solutions, even the initially μ values started to increase

immediately and continuously after the first a few laps along the sliding track.[16] A quick loss of lubricity of a monolayer of mucins in pin-on-disk tribometry, regardless of the type of mucin or pH, is ascribed to the weak physisorption nature of mucins via hydrophobic interaction between the terminal domains of mucins and PDMS surface. In turn, this also means that overall superior lubricating properties of BSM films to PGM films, as well as the improvement at pH 2.4 compared to pH 7.4 for both mucin films, are partly due to faster recovery of the lubricating mucin films as supplied from the bulk solution, following the continuous disrupt/removal from the PDMS surface under tribological stress.[59] Additionally, the faster kinetics of film formation can also explain the improved lubricity of PGM films at pH 2.4 than at pH 7.4 despite less amount and more viscous characteristics as mentioned above; more exposed hydrophobic moieties to solvent at the terminal regions at pH 2.4 facilitates faster adsorption onto PDMS surface and quicker formation of the lubricating films. Moreover, the suppressed electrostatic repulsion between neighbouring PGM molecules on nonpolar PDMS surface at pH 2.4 can further contribute to the PGM film stability, which is required for effective lubrication.

3.6 A proposed model for the hydrated film structures of the two mucins in aqueous solutions

The collective information obtained with an array of bulk and surface analytical techniques in this study showed that in aqueous environments both BSM and PGM spontaneously form films on PDMS surfaces, yet with fairly different hydrated film structures. A schematic illustration proposed for the BSM and PGM films on PDMS surface in aqueous solution at pH 7.4 and 2.4 is shown in Figure 6.

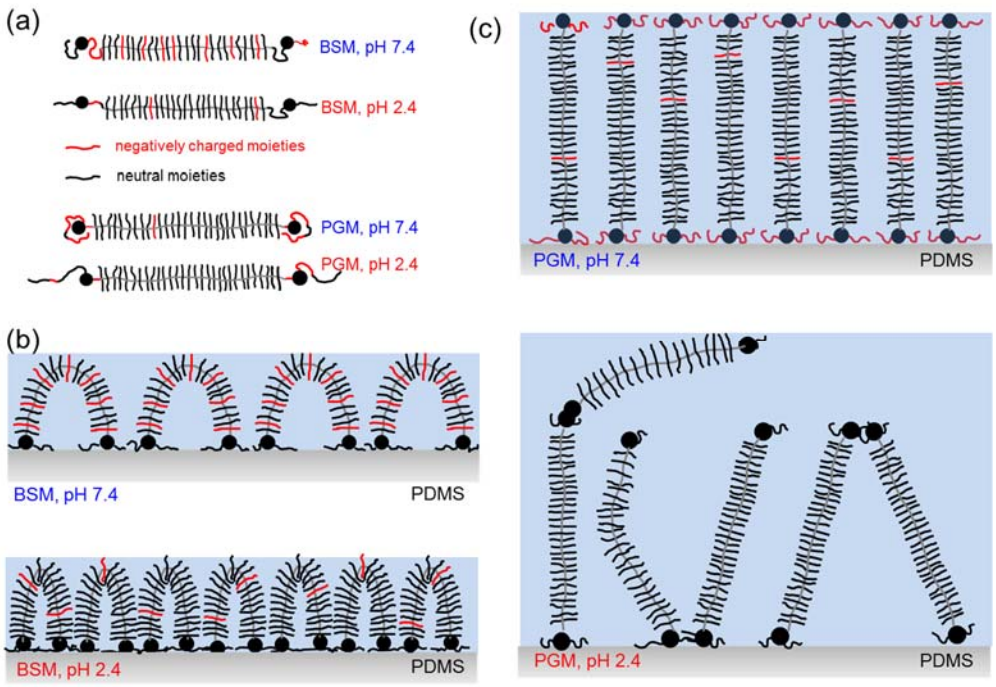

Figure 6. Schematic illustration of BSM and PGM films generated via spontaneous adsorption from aqueous solution onto PDMS surfaces in aqueous solutions at pH 7.4 and 2.4. The relative sizes of overall mucin molecules and its components are not to scale.

First of all, Figure 6(a) depicts schematics of molecular structures of BSM and PGM in bulk solution. Both mucins are relatively small and display "dumbbell"-like conformation rather than highly coiled conformation. In terms of size, BSM and PGM are roughly in a similar range of D_h (Figure 1) at pH 7.4 and both show a slight increase in D_h at pH 2.4. In terms of charge characteristics, while the two mucins revealed similar zeta potentials at both pH 7.4 and 2.4, the distribution of negatively charged moieties appears to be significantly different. Most importantly, the central glycosylated region of BSM is negatively charged due to the abundance of sialic acid moieties, whereas it is much less negatively charged because of the relative paucity of sialic acid moieties for PGM.[34,42] Thus, it is reasonable to assume that negative charges are present both in central and terminal regions for BSM, whereas a similar magnitude of negative

charges (Zeta potential in Figure 1) is localized at the terminal regions for PGM, although experimental verification on the distribution of charged moieties on the two types of mucins is necessary. Moreover, it is also proposed that the hydrophobic moieties are more buried in hydrophobic pockets, and possibly shielded by the negatively charged moieties in the case of PGM whereas hydrophobic patches of BSM are readily exposed to solvent even at pH 7.4.

The molecular structural difference between BSM and PGM critically affects the adsorption properties onto hydrophobic PDMS surface, both in terms of adsorption kinetics and conformation on the PDMS surface. For BSM (Figure 6(b)), as a compact film was formed with a small adsorbed mass at pH 7.4, we propose that 'loop'-like conformation is most dominant on PDMS surface. Meanwhile, higher adsorbed mass for PGM film at pH 7.4 can be explained by the dominance of 'tail'-like conformation (Figure 6(c)). Single-end anchoring of PGM on the surface is, however, not because either C- or N-terminal region of PGM has any particular preference to PDMS surface, but because the interaction of both termini with PDMS surface is generally less favourable and slower as discussed above. In a previous study employing arPGM,[15] poor lubricity at neutral pH despite high adsorbed mass was attributed to weakness of interaction between individual PGM molecules with PDMS substrate. This argument can be further substantiated by proposing that negatively charged moieties are localized at the terminal regions of PGM (Figure 6(c)) and consequent electrostatic repulsion between neighbouring PGM molecules on PDMS surfaces is a major source of film weakening factor. Moreover, requirement for PGM to rearrange its terminal region to expose hydrophobic moieties to interact with PDMS surface further delays facile adsorption onto PDMS surface both in adsorption kinetics and stability point of view. The two conformations exclusively illustrated for BSM and PGM films in Figure 6(b) and (c) are, of course, a highly simplified picture to emphasize the difference in

molecular structure of the two mucin films, and both conformations should be possible for both films at different ratios in reality.

A substantial increase in the adsorbed mass of BSM at pH 2.4 (Figure 3) may suggest a conformational change from 'loop' to 'tail' as with PGM. However, intensified elasticity of BSM films (Figure 4) indicates that the increased mass of BSM at pH 2.4 occurs via even more dense packing of BSM molecules without drastic conformational changes as illustrated in Figure 6(b). Overall, the acid-induced changes of BSM film structure conform to a conventional view for the adsorption of amphiphilic polyanionic macromolecules on nonpolar surfaces. Abnormal responses of PGM films as amphiphilic polyanion at acidic pH, such as reduced amount of adsorption and increased viscous characteristics, can also be related to the model that negative charges are localized at the terminal regions; the conformation of the central region, which occupies the majority of PGM molecule, is virtually not influenced by protonation of acidic moieties at low pH. Instead, the terminal regions of PGM may be linked with each other, as shown by the increase in D_h at pH 2.4 (Figure 1), following exposure of the hydrophobic patches to solvent. This may result in less effective packing and more loose structure, yet with higher amount of incorporated solvent as shown in Figure 6(c).

4. Conclusions

In this work, we have investigated and compared the structural and mechanical characteristics of mucin films generated from BSM and PGM by employing a variety of bulk and surface analytical techniques. An additional purification step was employed to remove the non-mucin proteins from PGM and BSM received from the commercial manufacturer. Furthermore, large aggregates or intrinsically large species of both mucins were also removed in this purification

step. Thus, the purified mucins were relatively small and homogeneous in hydrodynamic size distribution. Both mucins exhibited a fast spontaneous adsorption on hydrophobic PDMS surfaces from aqueous solutions. Films formed by the two types of mucins showed a number of important differences as well. Firstly, the formation of BSM films accompanied by the release of some portion of initially entrapped solvent, which indicates that a structural arrangement of BSM films occurred to result in a compact and elastic film conformation. This was well manifested in response to the lateral resonance by QCM-D. This behaviour was not observed from PGM films even though they incorporate even larger amounts of solvent. However, this does not necessarily mean higher affinity of water molecules to PGM films compared to BSM films, but rather implies that the network formed by PGM molecules on PDMS surface was more loose, resulting in the formation of more viscous films. This structural feature was most clearly manifested in the inferior lubricity of PGM films. Ultimately, the difference in the structural and mechanical properties of BSM and PGM films was correlated to the difference in the molecular structural of the two mucins. In particular, localized distribution of negatively charged motifs at the terminal regions and more buried location of hydrophobic patches for PGM can account for the formation of loose and weak film, which is not sufficient to withstand tribological stress.

Acknowledgements

European Research Council (ERC) is acknowledged for their financial support (Funding Scheme: ERC Starting Grant, 2010, Project Number 261152). Financial support from the Crafoord Foundation (grant 20140640) and from the Gustaf Th. Ohlsson Foundation is also acknowledged.

REFERENCES

(1) Desseyn, J. -L.; Tetaert, D.; Gouyer, V. Architecture of the Large Membrane-Bound Mucins. *Gene* **2008**, *410*, 215-222.
(2) Linden, S. K.; Sutton, P.; Karlsson, N. G.; Korolik, V.; McGuckin, M. A. Mucins in the Mucosal Barrier to Infection. *Mucosal. Immunol.* **2008**, *1*, 183-197.
(3) Roussel, P.; Delmotte, P. The Diversity of Epithelial Secreted Mucins. *Curr. Org. Chem.* **2004**, *8*, 413-437.
(4) Svensson, O.; Arnebrant, T. Mucin layers and multilayers: Physicochemical Properties and Applications. *Curr. Opinion Colloid Interf. Sci.* **2010**, *15*, 395-405.
(5) Thornton, D. J.; Rousseau, K.; McGuckin, M. A. Structure and Function of the Polymeric Mucins in Airways Mucus. *Ann. Rev. Physiol.* **2008**, *70*, 459-486.
(6) Hattrup, C. L.; Gendler, S. J. Structure and Function of the Cell Surface (Tethered) Mucins. *Ann. Rev. Physiol.* **2008**, *70*, 431-457.
(7) Shi, L.; Caldwell, K. D. Mucin Adsorption to Hydrophobic Surfaces. *J. Colloid. Interf. Sci.* **2000**, *224*, 372-381.
(8) Bushnak, I. A.; Labeed, F. H.; Sear, R. P.; Keddie, J. L. Adhesion of Microorganisms to Bovine Submaxillary Mucin Coatings: Effect of Coating Deposition Conditions. *Biofouling* **2010**, *2*, 387-397.
(9) Sandberg, T.; Carlsson, J.; Ott, M. K. Mucin Coatings Suppress Neutrophil Adhesion to a Polymeric Model Biomaterial. *Microscopy Res. Tech.* **2007**, *70*, 864-868.
(10) Shi, L.; Ardehali, R.; Caldwell, K. D.; Valint, P. Mucin Coating on Polymeric Material Surfaces to Suppress Bacterial Adhesion. *Colloids Surf. B: Biointerfaces* **2000**, *17*, 229-239.
(11) Shi, L.; Ardehali, R.; Valint, P.; Caldwell, K. Bacterial Adhesion to a Model Surface with Self-generated Protection Coating of Mucin via Jacalin. *Biotechnol. Lett.* **2001**, *23*, 437-441.
(12) Iijima, M.; Yoshimura, M.; Tsuchiya, T.; Tsukada, M.; Ichikawa, H.; Fukumori, Y.; Kamiya, H. Direct Measurement of Interactions between Stimulation-Responsive Drug Delivery Vehicles and Artificial Mucin Layers by Colloid Probe Atomic Force Microscopy. *Langmuir* **2008**, *24*, 3987-3992.
(13) Harvey, N. M.; Yakubov, G. E.; Stokes, J. R.; Klein, J. Normal and Shear Forces between Surfaces Bearing Porcine Gastric Mucin, a High-Molecular-Weight Glycoprotein. *Biomacromolecules* **2011**, *12*, 1041-1050.
(14) Yakubov, G. E.; McColl, J.; Bongaerts, J. H. H.; Ramsden, J. J. Viscous Boundary Lubrication of Hydrophobic Surfaces by Mucin. *Langmuir* **2009**, *25*, 2313-2321.
(15) Lee, S.; Müller, M.; Rezwan, K.; Spencer, N. D. Porcine Gastric Mucin (PGM) at the Water/Poly(dimethylsiloxane) (PDMS) Interface: Influence of pH and Ionic Strength on Its Conformation, Adsorption, and Aqueous Lubrication Properties. *Langmuir* **2005**, *21*, 8344-8353.
(16) Nikogeorgos, N.; Madsen, J. B.; Lee, S. Influence of Impurities and Contact Scale on the Lubricating Properties of Bovine Submaxillary Mucin (BSM) Films on a Hydrophobic Surface. *Colloids Surf. B: Biointerfaces* **2014**, *122*, 760-766.

(17) Nikogeorgos, N.; Efler, P.; Kayitmazer, A. B.; Lee, S. "Bio-glues" to Enhance Slipperiness of Mucins: Improved Lubricity and Wear Resistance of Porcine Gastric Mucin (PGM) Layers Assisted by Mucoadhesion with Chitosan. *Soft Matter* **2015**, *11*, 489-498.
(18) Çelebioğlu, H. Y; Gudjónsdóttir, M.; Chronakis, I. S.; Lee, S. Investigation of the Interaction between Mucins and β-lactoglobulin under Tribological Stress. *Food Hydrocolloids* **2016**, *54*, 57-65.
(19) Madsen, J. B.; Pakkanen, K. I.; Duelund, L.; Svensson, B.; Abou Hachem, M.; Lee, S. A Simplified Chromatographic Approach to Purify Commercially Available Bovine Submaxillary Mucins (BSM). *Prep. Biochem. Biotechnol.* **2015**, *45*, 84-99.
(20) Lundin, M.; Sandberg, T.; Caldwell, K.D.; Blomberg, E. Comparison of the Adsorption Kinetics and Surface Arrangement of "As Received" and Purified Bovine Submaxillary Gland Mucin (BSM) on Hydrophilic Surfaces. *J. Colloid Interf. Sci.* **2009**, *336*, 30-39.
(21) Røn, T.; Javakhishvili, I.; Jankova, K.; Hvilsted, S.; Lee, S. Adsorption and Aqueous Lubricating Properties of Charged and Neutral Amphiphilic Diblock Copolymers at a Compliant, Hydrophobic Interface. *Langmuir* **2013**, *29*, 7782-7792.
(22) Ramsden, J. J. Review of New Experimental Techniques for Investigating Random Sequential Adsorption. *J. Stat. Phys*. **1993**, *73*, 853-877.
(23) Bettelheim, F. A.; Dey, S. K. Molecular Parameters of Submaxillary Mucins. *Arch. Biochem. Biophys.* **1965**, *109*, 259-265.
(24) Rodahl, M.; Hook, F.; Fredriksson, C.; A. Keller, C.; Krozer, A.; Brzezinski, P.; Voinova, M.; Kasemo, B. Simultaneous Frequency and Dissipation Factor QCM Measurements of Biomolecular Adsorption and Cell Adhesion. *Faraday Discuss.* **1997**, *107*, 229-246.
(25) Sauerbrey, G. Verwendung von Schwingquarzen zur Wägung dünner Schichten und zur Mikrowägung. *Z. Physik* **1959**, *155*, 206-222.
(26) Reviakine, I., Johannsmann D.; Richter, R. P. Hearing What You Cannot See and Visualizing What You Hear: Interpreting Quartz Crystal Microbalance Data from Solvated Interfaces. *Anal. Chem.* **2011**, *83*, 8838-8848.
(27) Höök, F.; Kasemo, B.; Nylander, T.; Fant, C.; Sott, K.; Elwing, H. Variations in Coupled Water, Viscoelastic Properties, and Film Thickness of a Mefp-1 Protein Film during Adsorption and Cross-Linking: A Quartz Crystal Microbalance with Dissipation Monitoring, Ellipsometry, and Surface Plasmon Resonance Study. *Anal. Chem.* **2011**, *73*, 5796-5804.
(28) Sotres, J.; Barrantes, A.; Lindh, L.; Arnebrant, T. Strategies for a Direct Characterization of Phosphoproteins on Hydroxyapatite Surfaces. *Caries Res.* **2014**, *48*, 98-110.
(29) Voinova, M. V.; Rodahl, M.; Jonson, M.; Kasemo, B. Viscoelastic Acoustic Response of Layered Polymer Films at Fluid-Solid Interfaces: Continuum Mechanics Approach. **1999**, *Phys. Scr.*, *59*, 391-396.
(30) Tsortos, A.; Papadakis, G.; Gizeli, E. Shear Acoustic Wave Biosensor for Detecting DNA Intrinsic Viscosity and Conformation: A Study with QCM-D. *Biosens. Bioelectron.* **2008**, *24*, 836-841.

(31) Zappone, B.; Patil, N. J.; Madsen, J. B.; Pakkanen, K. I.; Lee, S. Molecular Structure and Equilibrium Forces of Bovine Submaxillary Mucin Adsorbed at a Solid–Liquid Interface, *Langmuir* **2015**, *31*, 4524-4533.
(32) Claesson, P. M.; Blomberg, E.; Fröberg, J. C.; Nylander, T.; Arnebrant, T. Protein Interactions at Solid Surfaces. *Adv. Colloid Interf. Sci.* **1995**, *57*, 161-227.
(33) Malmsten, M.; Blomberg, E.; Claesson, P.; Carlstedt, I.; Ljusegren, I. Mucin Layers on Hydrophobic Surfaces Studied with Ellipsometry and Surface Force Measurements, *J. Colloid Interf. Sci.* **1992**, *151(2)*, 579-590.
(34) Yakubov, G. E.; Papagiannopoulos, A; Rat, E.; Easton, R.L.; Waigh, T. A. Molecular structure and rheological properties of short-side-chain heavily glycosylated porcine stomach mucin. *Biomacromolecules* **2007**, *8*, 3467-3477.
(35) Di Cola, E; Yakubov, G. E.; Waigh, T. A. Double-Globular Structure of Porcine Stomach Mucin: A Small-Angle X-ray Scattering Study. *Biomacromolecules* **2008**, *11*, 3216-3222.
(36) Cao, X.; Bansil, R.; Bhaskar, K. R.; Turner, B. S.; LaMont, J. T.; Niu, N.; Afdhal, N. H. pH-Dependent Conformational Change of Gastric Mucin Leads to Sol-Gel Transition. *Biophys. J.* **1999**, *76*, 1250-1258.
(37) Thomsson, K. A.; Karlsson, N. G.; Hansson, G. C. Liquid Chromatography–Electrospray Mass Spectrometry as a Tool for the Analysis of Sulfated Oligosaccharides from Mucin Glycoproteins. *J. Chromatography A* **1999**, *854*, 131-139.
(38) Karlsson, N. G.; Packer, N. H. Analysis of *O*-linked Reducing Oligosaccharides Released by an In-line Flow System. *Anal. Biochem.* **2002**, *305*, 173-185.
(39) Karlsson, N. G.; Nordman, H.; Karlsson, H.; Carlstedt, I.; Hansson, G. C. Glycosylation Differences between Pig Gastric Mucin Populations: A Comparative Study of the Neutral Oligosaccharides Using Mass Spectrometry. *Biochem. J.* **1997**, *326*, 911-917.
(40) Mikuni-Takagaki, Y.; Hotta, K. Characterization of Peptic Inhibitory Activity Associated with Sulfated Glycoprotein Isolated from Gastric Mucosa. *Biochimica et Biophysica Acta (BBA)* **1979**, *584*, 288-297.
(41) Tettamanti, G.; Pigman, W. Purification and Characterization of Bovine and Ovine Submaxillary Mucins. *Arch. Biochem. Biophys.* **1968**, *124*, 41-50.
(42) Sandberg, T.; Blom, H.; Caldwell, K.D. Potential Use of Mucins as Biomaterial Coatings I. Fractionation, Characterization, and Model Adsorption of Bovine, Porcine, and Human Mucins. *J. Biomed. Mater. Res. A*. **2009**, *91*, 762-772.
(43) Yang, J. T.; Wu, C. S. C.; Böhm, G. Circular dichroism (CD) Parameters and Secondary Structure Estimates of Proteins. In Structural and Physical Data I, Hinz, H. J., Ed.; Springer Berlin Heidelberg, **2003**; Vol. 2a, pp. 7001-7018.
(44) Kelly, S. M.; Jess, T. J.; Price, N. C. How to Study Proteins by Circular Dichroism. *Biochim. Biophys. Acta.* **2005**, *1751*, 119-139.
(45) Ambort, D.; Johansson, M. E. V.; Gustafsson, J. K.; Nilsson, H. E.; Ermund, A.; Johansson, B. R.; Koeck, P. J. B.; Hebert, H.; Hansson, G. C. Calcium and pH-Dependent Packing and Release of the Gel-forming MUC2 mucin. *Proc. Natl. Acad. Sci.* **2012**, *109*, 5645-5650.

(46) Pigman, W.; Moschera, J.; Weiss, M.; Tettamanti, G. The Occurrence of Repetitive Glycopeptide Sequences in Bovine Submaxillary Glycoprotein. *Eur. J. Biochem.* **1973**, *32*, 148-154.
(47) Dekker, J.; Rossen, J. W. A.; Büller, H. A.; Einerhand, A. W. C. The MUC Family: An Obituary. *Trends Biochem. Sci.* **2002**, *27*, 126-131.
(48) Perez-Vilar, J.; Eckhardt, A. E.; DeLuca, A.; Hill, R. L. Porcine Submaxillary Mucin Forms Disulfide-Linked Multimers through Its Amino-Terminal D-domains. *J. Biol. Chem.* **1998**, *273*, 14442-14449.
(49) Perez-Vilar, J.; Hill, R. L. The Structure and Assembly of Secreted Mucins. *J. Biol. Chem.* **1999**, *274*, 31751-31754.
(50) Sreerama, N.; Woody, R. W. Poly(Pro) II Helixes in Globular Proteins: Identification and Circular Dichroic Analysis. *Biochemistry* **1994**, *33*, 10022-10025.
(51) Adzhubei, A. A.; Sternberg, M. J. E.; Makarov, A. A. Polyproline-II Helix in Proteins: Structure and Function. *J. Mol. Biol.* **2013**, *425*, 2100-2132.
(52) Voet, D.; Voet, J. G. Three-Dimensional Structures of Proteins. In Biochemistry, 3rd ed.; John Wiley & sons, **2004**, pp. 219-227.
(53) Sotres, J.; Madsen, J. B.; Arnebrant, T.; Lee, S. Adsorption and Nanowear Properties of Bovine Submaxillary Mucin Films on Solid Surfaces: Influence of Solution pH and Substrate Hydrophobicity. *J. Colloid Interf. Sci.* **2014**, *428*, 242-250.
(54) Stuart, M. A. C.; Hoogendam, C. W.; Keizer, A. d. Kinetics of Polyelectrolyte Adsorption. *J. Physics: Condensed Matter* **1997**, *9*, 7767-7783.
(55) Abraham, T.; Giasson, S.; Gohy, J. F.; Jérôme, R.; Müller, B.; Stamm, M. Adsorption Kinetics of a Hydrophobic−Hydrophilic Diblock Polyelectrolyte at the Solid−Aqueous Solution Interface: A Slow Birth and Fast Growth Process. *Macromolecules* **2000**, *33*, 6051-6059.
(56) An, J.; Dédinaite, A.; Nilsson, A.; Holgersson, J.; Claesson, P. M. Comparison of a Brush-with-Anchor and a Train-of-Brushes Mucin on Poly(methyl methacrylate) Surfaces: Adsorption, Surface forces, and Friction. *Biomacromolecules* **2014**, *15*, 1515-1525.
(57) Halthur, T. J.; Arnebrant, T.; Macakova, L.; Feiler, A. Sequential Adsorption of Bovine Mucin and Lactoperoxidase to Various Substrates Studied with Quartz Crystal Microbalance with Dissipation. *Langmuir* **2010**, *26*, 4901-4908.
(58) Müller, M. T.; Yan, X.; Lee, S.; Perry, S. S.; Spencer, N.D. Lubrication Properties of a Brush-like Copolymer As a Function of the Amount of Solvent Absorbed within the Brush. *Macromolecules* **2005**, *38*, 5706-5713.
(59) Lee, S.: Müller, M.; Heeb, R.; Zürcher, S.; Tosatti, S.; Heinrich, M.; Amstad, F.; Pechmann, S.; Spencer, N.D. Self-Healing Behavior of a Polyelectrolyte-Based Lubricant Additive for Aqueous Lubrication of Oxide Materials. *Tribol. Lett*. **2006**, *24*, 217-223.